STABILITY ANALYSIS OF FLOCK AND MILL RINGS FOR 2ND ORDER MODELS IN SWARMING

G. ALBI[1], D. BALAGUÉ[2], J. A. CARRILLO[3] AND J. VON BRECHT[4]

Abstract. We study the linear stability of flock and mill ring solutions of two individual based models for biological swarming. The individuals interact via a nonlocal interaction potential that is repulsive in the short range and attractive in the long range. We relate the instability of the flock rings with the instability of the ring solution of the first order model. We observe that repulsive-attractive interactions lead to new configurations for the flock rings such as clustering and fattening formation. Finally, we numerically explore mill patterns arising from this kind of interactions together with the asymptotic speed of the system.

1. Introduction

Individual-based models (IBMs) appear in biology, mathematics, physics, and engineering. They describe the motion of a collection of N individual entities, so the system is defined on a microscopic scale. IBMs are good models for some applications when the number of particles is reasonable. Nonetheless, when the number is large, it is more reasonable to use a continuum model. Some continuum models, like the one in [13, 12], are derived as a mean-field particle limit leading to a mesoscopic kinetic description of the problem. At this level, one looks at the probability density of finding particles at a certain position and velocity at a given time. Several models have been proposed to describe the flocking of birds [8, 28, 4, 27], the formation of ant trails [18], the schooling of fish [21, 7, 5], swarms of bacteria [23], etc.

These models can include some rules that describe the behavior of each individual of the system. Such mechanisms can help to describe the influence of each individual on the others, depending on their relative position and velocity. For instance, one example is the classical three zone model [1, 22]. A three zone model describes how social the individual is in the following sense. If two individuals are too close, they want to have their own space (repulsion). When one individual is far from the group, it wants to go back and socialize (attraction). And finally, in the group, each individual tries to mimic the behavior of the others (orientation). Other models just consider rules for orientation, like the Vicsek model [29, 16]. In this case, there is a mechanism of self-propulsion in which each individual moves with constant speed and adopts the average direction among their local neighbors.

We focus our study in the analysis of two particular examples of IBMs. The first one is a self-propelled interacting particle model that was introduced in [26] and extensively studied

DB and JAC were partially supported by the project MTM2011-27739-C04-02 DGI (Spain) and 2009-SGR-345 from AGAUR-Generalitat de Catalunya. JAC acknowledges support from the Royal Society through a Wolfson Research Merit Award. GA acknowledges support from the Università di Ferrara through "Fondi cinque per mille, anno 2009". JvB acknowledges funding from NSF grant EFRI-1024765 and NSF grant DMS-0907931. This work was supported by Engineering and Physical Sciences Research Council grant number EP/K008404/1.

in [17, 13]:

$$\begin{cases} \dot{x}_j = v_j \\ \dot{v}_j = S(|v_j|)v_j + \dfrac{1}{N}\displaystyle\sum_{\substack{l=1 \\ l\neq j}}^{N} \nabla W(x_l - x_j) \end{cases} \quad , \quad j = 1, \dots, N \tag{1}$$

We are going to consider the same *self-propulsion/ friction* term used in [17, 13],

$$S(|v_j|) = \alpha - \beta |v_j|^2, \qquad \alpha, \beta > 0.$$

Note that such a term gives us an asymptotic speed for the particles, equal to $\sqrt{\alpha/\beta}$. In these references, the authors study (1) with pairwise interaction given by the so-called Morse potential

$$U(r) = C_A e^{-r/l_A} - C_R e^{-r/l_R},$$

with C_A, C_R denoting the attractive and repulsive strengths and l_A, l_R their respective length scales. They find and describe several patterns for the asymptotic behavior in 2D. They observed flocking behavior, mill on a ring, and clustering when particles are milling. In [9], a well-posedness theory is developed for (1) proving the mean-field limit under smoothness assumptions on the potential. The authors show convergence of the particle model toward a measure solution of the kinetic equation.

We perform an analysis on the stability of flock rings and the mill rings as asymptotic solutions for (1). The ring solution was recently studied in [25, 6] where the authors in this work do a careful general linear analysis of the rings for the first order model

$$\dot{X}_j = \sum_{\substack{l=1 \\ l\neq j}}^{N} \nabla W\left(X_j - X_l\right), \quad j = 1, \dots, N. \tag{2}$$

Part of the analysis of (2) is used to study the the stability of mill rings in (1), described in [17]. Related pattern formation in the associated first order model has been studied in [30, 24].

Another second order model that we are going to study is

$$\begin{cases} \dot{x}_j = v_j \\ \dot{v}_j = \dfrac{1}{N}\displaystyle\sum_{l=1}^{N} H(x_j - x_l)(v_l - v_j) + \dfrac{1}{N}\sum_{\substack{l=1 \\ l\neq j}}^{N} \nabla W(x_l - x_j) \end{cases} \quad , \quad j = 1, \dots, N \tag{3}$$

with $x_j, v_j \in \mathbb{R}^2$ where the velocity v_j is described by the Cucker-Smale alignment term H and the pairwise interaction by a repulsive-attractive radial potential $W(x) = k(|x|)$.

Even if the analysis has been done in full generality for the parameter functions of the model H and W, we will emphasize the results in some relevant cases. For instance, we consider the case of power law repulsive-attractive potentials [25, 3]

$$k(r) = \frac{r^a}{a} - \frac{r^b}{b}, \qquad a > b > 0. \tag{4}$$

For the Cucker-Smale alignment [14, 15, 20, 19, 10], a relevant case is $H(x) = g(|x|)$ with

$$g(r) = \frac{1}{(1 + r^2)^\gamma}, \qquad \gamma > 0.$$

The main results of this work show that the flock ring is unstable in the second order models (1) and (3) if and only if its spatial shape is unstable in the first order model (2). We use the same kind of strategy as in [6].

The main idea is to study the stability of the system of ODEs (1) by analyzing the eigenvalues of a suitable linearization with restricted perturbations. We consider particular perturbations of the flock rings in such a way that translational invariance is avoided while preserving the mean velocity. This is really needed since the linearized system associated to (1) is always linearly unstable due to translations. Translational invariance implies the existence of a generalized eigenvector associated to the zero eigenvalue of the matrix defining the linearized system. We characterize all cases in which the linearized system has eigenvalues with zero real part and their consequences in the instability condition. An analysis of the stability of the family of flock solutions is under way in [11].

In addition to flock rings, other spatial shapes are possible as asymptotic solutions. One can also observe flocks on annuli (fattening), lines or points (clustering). These patterns can be explained due to the results in [2].

For the mill ring analysis, we start from the results of [6] to explore other mill configurations that appear with repulsive-attractive potentials. We numerically investigate the formation of fat mills due to the repulsive force and the formation of clusters when varying the asymptotic speed. In addition, we show some switching behaviors between flock and mill rings.

The structure of the paper is as follows. In Section 2 we study the microscopic and the mesoscopic models and we give the definitions of the main objects in our studies, the flock and mill rings. In Section 3 we do a linear stability analysis on the flock rings for models (1) and (3). We also explore the fattening and cluster formation. Finally, in Section 4 we do a similar study on the stability for mill rings. In all sections we have performed several numerical tests supporting our theoretical results.

2. Microscopic & Mesoscopic models

Let us introduce some particular solutions of the particle model (1) and its continuum counterpart.

2.1. Flock and mill solutions: microscopic model.

Definition 1. *We call a* flock ring*, the solution of* (1) *such that* $\{x_j\}_{j=1}^N$ *are equally distributed on a circle with a certain radius,* R *and* $\{v_j\}_{j=1}^N = u_0$*, with* $|u_0| = \sqrt{\alpha/\beta}$*.*

Definition 2. *We call a* mill ring*, the solution of* (1) *such that* $\{x_j\}_{j=1}^N$ *are equally distributed on a circle with a certain radius,* R *and* $\{v_j\}_{j=1}^N = u_j^0 = \sqrt{\alpha/\beta}\, x_j^\perp/|x_j|$ *with* $x_j^\perp$ *the orthogonal vector.*

By abuse of notation, we will write $|u_0|$ for $\left|u_j^0\right|$ since $\left|u_j^0\right| = \sqrt{\alpha/\beta}$ for all $j = 1, \dots, N$. Moreover, we will make use of notation $|u_0|$ for both flock and mill rings indistinctly.

All over the paper, we will identify $e^{i\theta} \equiv (\cos\theta, \sin\theta)$ and use x to identify the vector and the complex numbers indistinctly

$$x_j(t) = R\left(\cos\left(\frac{2\pi}{N}j + \omega t\right), \sin\left(\frac{2\pi}{N}j + \omega t\right)\right) = Re^{i\frac{2\pi j}{N}} e^{i\omega t}. \tag{5}$$

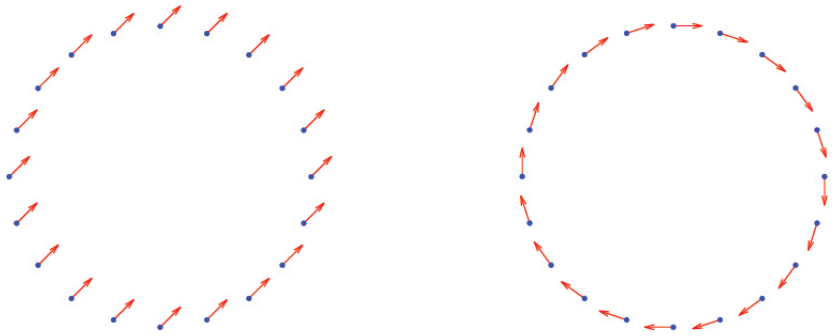

FIGURE 1. Flock and mill ring solutions.

In the case of mill rings, we are looking for a solution of the form (5). The case of a flock ring in the comoving frame is equivalent to looking for a solution of the form (5) with $\omega = 0$. Plugging (5) into (1), we obtain

$$\sum_{\substack{l=1\\ l\neq j}}^{N} \nabla W(x_j - x_l) = 0;$$

therefore, R is determined only by the repulsive-attractive potential.

In the case of mill rings, we have

$$v_j(t) = \dot{x}_j(t) = R\omega i e^{i\theta_j} e^{i\omega t}, \quad \theta_j = \frac{2\pi j}{N},$$

and thus, $R^2\omega^2 = \frac{\alpha}{\beta}$. Moreover, by taking the derivative

$$\dot{v}_j = -\omega^2 x_j = -\omega^2 \frac{1}{N} \sum_{\substack{l=1\\ l\neq j}}^{N} (x_l - x_j) = 0.$$

Plugging this into (1), we get

$$\sum_{\substack{l=1\\ l\neq j}}^{N} \left[\nabla W(x_l - x_j) - \omega^2 (x_l - x_j)\right] = \sum_{\substack{l=1\\ l\neq j}}^{N} \nabla \tilde{W}(x_l - x_j) = 0,$$

with $\tilde{W}(x) = W(x) - \omega^2 \frac{|x|^2}{2}$. Thus in order to find the radius for flock and mill rings, we need to solve the same equation. This expression implies that the spatial shape has to balance attraction versus repulsion and centrifugal forces. Now, a direct computation yields

$$|x_j - x_l| = 2R \sin\left(\frac{(l-j)\pi}{N}\right)$$

for all times. One can easily compute that

$$x_l - x_j = 2R \sin\left(\frac{p\pi}{N}\right) \begin{pmatrix} -\sin\left(\frac{p\pi}{N}\right) & \cos\left(\frac{p\pi}{N}\right) \\ \cos\left(\frac{p\pi}{N}\right) & \sin\left(\frac{p\pi}{N}\right) \end{pmatrix} \begin{pmatrix} \cos(\theta_j) \\ \sin(\theta_j) \end{pmatrix}, \quad p = l - j,$$

and

$$\sum_{\substack{l=1\\ l\neq j}}^{N}\nabla\tilde{W}(|x_j-x_l|)=\sum_{\substack{l=1\\ l\neq j}}^{N}(x_j-x_l)\frac{\tilde{k}'(|x_j-x_l|)}{|x_j-x_l|}$$
$$=\sum_{\substack{l=1\\ l\neq j}}^{N}\begin{pmatrix}-\sin\left(\frac{p\pi}{N}\right)\cos\left(\theta_j\right)+\cos\left(\frac{p\pi}{N}\right)\sin\left(\theta_j\right)\\ \\ \cos\left(\frac{p\pi}{N}\right)\cos\left(\theta_j\right)+\sin\left(\frac{p\pi}{N}\right)\sin\left(\theta_j\right)\end{pmatrix}\tilde{k}'(|x_j-x_l|).$$

By symmetry we can assume $j=N$, and thus

$$\sum_{\substack{l=1\\ l\neq j}}^{N}\nabla\tilde{W}(|x_j-x_l|)=\sum_{p=1}^{N-1}\begin{pmatrix}-\sin\left(\frac{p\pi}{N}\right)\\ \\ \cos\left(\frac{p\pi}{N}\right)\end{pmatrix}\tilde{k}'(|x_j-x_l|),$$

changing j to $N-j$, we finally obtain

$$\sum_{\substack{l=1\\ l\neq j}}^{N}\nabla\tilde{W}(|x_j-x_l|)=\begin{pmatrix}-\sum_{p=1}^{N-1}\sin\left(\frac{p\pi}{N}\right)\tilde{k}'\left(2R\sin\left(\frac{p\pi}{N}\right)\right)\\ \\ 0\end{pmatrix}. \tag{6}$$

As a conclusion, the radius of a flock or mill ring solution is characterized by

$$\sum_{p=1}^{N-1}\sin\left(\frac{p\pi}{N}\right)\tilde{k}'\left(2R\sin\left(\frac{p\pi}{N}\right)\right)=0.$$

For general potentials there can be more than one flock or mill solution. In the case of the power law potentials (4), there is only one solution. Condition (6) reads

$$(2R)^{a-1}\frac{1}{N}\sum_{p=0}^{N-1}\sin^a\left(\frac{p\pi}{N}\right)-(2R)^{b-1}\frac{1}{N}\sum_{p=0}^{N-1}\sin^b\left(\frac{p\pi}{N}\right)-2R\omega^2\frac{1}{N}\sum_{p=0}^{N-1}\sin^2\left(\frac{p\pi}{N}\right)=0. \tag{7}$$

To prove uniqueness, we notice that the function $f(r)=C_1r^a-C_2r^b-C_3$ with $a>b>0$ and $C_1>C_2>0$, $C_3>0$, has only one zero. Computing the first derivative and looking for critical points, we obtain $r_1=0$ and $r_2^{a-b}=\frac{C_2b}{C_1a}$. Taking the second derivative and evaluating at r_2, one obtains $f''(r_2)=r_2^{b-2}C_2b(a-b)>0$, so r_2 is a local minimum. For $0<r<r_2$, one has $f'(r)<0$ whereas for all $r\in(r_2,+\infty)$, one has $f'(r)>0$. Then we conclude that $f(r)$ has a unique zero. Notice that the solution to (7) depends on the number of particles and we will use the notation $R=R(N)$.

2.2. **Flock and mill solutions: mesoscopic model.** In this subsection we characterize the radius of flock and mill rings. We introduce the function

$$\psi_\alpha(s)=\frac{1}{\pi}\int_0^\pi(1-s\cos\theta)(1+s^2-2s\cos\theta)^{\frac{\alpha-2}{2}}\,d\theta,$$

already analyzed in [3]. A change of variables in the previous function shows that

$$\psi_\alpha(1)=\frac{2^{\alpha-1}}{\pi}B\left(\frac{\alpha+1}{2},\frac{1}{2}\right). \tag{8}$$

Lemma 1. *If $N \to \infty$ then $R(N) \to R_{ab}(|u_0|)$ where $R_{ab}(|u_0|)$ is the solution of the following equation:*

$$\psi_a(1)R^{a-1} - \psi_b(1)R^{b-1} - \omega^2 R = 0.$$

Proof. We first take $2^{a-1}\frac{1}{N}\sum_{p=0}^{N-1}\sin^a(\frac{p\pi}{N})$. Multiplying and dividing by π we obtain the following equality

$$\lim_{N\to\infty} 2^{a-1}\frac{1}{\pi}\left(\frac{\pi}{N}\sum_{p=0}^{N-1}\sin^a\left(\frac{p\pi}{N}\right)\right) = 2^{a-1}\frac{1}{\pi}\int_0^{\pi}\sin^a(x)\,dx = 2^{a-1}\frac{1}{\pi}\left(2\int_0^{\pi/2}\sin^a(x)\,dx\right). \quad (9)$$

Now, we use the following expression for the Beta function

$$B(x,y) = 2\int_0^{\pi/2}(\cos\theta)^{2x-1}(\sin\theta)^{2y-1}\,d\theta,$$

with $x = \frac{1}{2}$, $y = \frac{a+1}{2}$, and using that $B(x,y) = B(y,x)$ in (9) together with (8) to obtain

$$\lim_{N\to\infty} 2^{a-1}\frac{1}{\pi}\left(\frac{\pi}{N}\sum_{p=0}^{N-1}\sin^a\left(\frac{p\pi}{N}\right)\right) = 2^{a-1}\frac{1}{\pi}B\left(\frac{a+1}{2},\frac{1}{2}\right) = \psi_a(1).$$

The same reasoning works by changing a for b in the second term in (7). For the third term we use the fact that we can compute the exact sum

$$\frac{2}{N}\sum_{p=0}^{N-1}\sin^2\left(\frac{p\pi}{N}\right) = 1.$$

□

Remark 1. *In the case of flock rings $\omega = 0$, their radius is determined by the radius of the aggregation ring found in* [3]

$$R(N) \to R_{ab} = \frac{1}{2}\left(\frac{B(\frac{b+1}{2},\frac{1}{2})}{B(\frac{a+1}{2},\frac{1}{2})}\right)^{\frac{1}{a-b}} \quad as \quad N\to\infty.$$

Remark 2. *Let $W(x) = k(|x|)$ be a general interaction potential. Call $f(r) = -k'(r)/r$. Then the radius of the ring is determined by*

$$\int_0^{\frac{\pi}{2}} f(2R\sin(\theta))\sin^2(\theta)\,d\theta = 0,$$

as shown in [6].

Remark 3. *The corresponding mesoscopic model to the particle system* (1)*, as proven in* [9]*, is given by the kinetic equation*

$$\frac{\partial f}{\partial t} + v\cdot\nabla_x f + \mathrm{div}_v[(\alpha - \beta|v|^2)vf)] - \mathrm{div}_v[(\nabla_x W * \rho)f] = 0, \quad (10)$$

where

$$\rho(t,x) = \int_{\mathbb{R}^2} f(t,x,v)\,dv.$$

It was shown in [12] *that singular solutions of the type*

$$f(t,x,v) = \rho(t,x)\delta\left(v - u_0\right), \qquad f(t,x,v) = \rho(t,x)\delta\left(v - \sqrt{\frac{\alpha}{\beta}}\frac{x^{\perp}}{x}\right),$$

with $\rho(t,x)$ the uniform distribution on a ring, are weak solutions of the kinetic model (10)*, called the flock and mill ring continuous solutions respectively.*

3. Linear stability analysis for flock rings

We will now focus on the stability analysis of flock rings for some particular perturbations in terms of the parameters of the model (a, b, u_0). We take advantage of the careful stability analysis of the ring solutions of the aggregation equation performed in [6].

3.1. **Stability of flock solutions without the Cucker-Smale term.** We consider the model (1) and we perform the change of variables to the comoving frame

$$\begin{cases} y_j(t) = x_j(t) - u_0 t \\ z_j(t) = v_j(t) - u_0 \end{cases} \qquad j = 1, \dots, N, \tag{11}$$

where u_0 is the asymptotic velocity of a fixed flock ring. Therefore the system (1) reads

$$\begin{cases} \dfrac{d}{dt} y_j = v_j - u_0 = z_j \\ \dfrac{d}{dt} z_j = \underbrace{(\alpha - \beta |z_j + u_0|^2)}_{S_0(|z_j|)} (z_j + u_0) - \dfrac{1}{N} \displaystyle\sum_{\substack{k=1 \\ k \neq j}}^{N} \nabla W(y_j - y_k) \end{cases} , \quad j = 1, \dots, N.$$

A flock ring can then be characterized as a stationary solution of the form $\left(y_j^0, z_j^0\right) = \left(Re^{i\theta_j}, 0\right)$, where $\theta_j = \frac{2\pi j}{N}$ for $j = 1, \dots, N$. This stationary solution satisfies

$$S_0(|z_j^0|) = 0, \quad \nabla S_0(|z_j^0|) = -2\beta u_0 u_0^*, \quad 0 = \sum_{k \neq j} k'(|y_j^0 - y_k^0|) \frac{(y_k^0 - y_j^0)}{|y_k^0 - y_j^0|}.$$

As in [6], we restrict the set of possible perturbations of the flock solution to those of the form

$$\tilde{y}_j(t) = Re^{i\theta_j}(1 + h_j(t)),$$

where $h_j \in \mathbb{C}$, such that $|h_j| \ll 1$ and

$$\sum_{j=1}^{N} h_j(t) = \sum_{j=1}^{N} h_j'(t) = 0. \tag{12}$$

The first restriction is to avoid the zero eigenvalue due to translations. The second one comes from the fact that the mean velocity of the perturbed system should be u_0. More general perturbations will generically lead to other flock solutions with different asymptotic velocity u_0. Their orbital stability will be analyzed elsewhere [11]. Therefore, the perturbed system reads

$$\begin{cases} \dfrac{d}{dt} \tilde{y}_j(t) = Re^{i\theta_j} h_j' = \tilde{z}_j \\ \dfrac{d}{dt} \tilde{z}_j(t) = Re^{i\theta_j} h_j'' = S_0(|\tilde{z}_j|) - \dfrac{1}{N} \displaystyle\sum_{\substack{l=1 \\ l \neq j}}^{N} \nabla W(\tilde{y}_j - \tilde{y}_l) \end{cases} , \quad j = 1, \dots, N.$$

The linearization of the system around the flock solution (y_j^0, z_j^0) reads as

$$\begin{cases} \dfrac{d}{dt}\tilde{y}_j(t) = Re^{i\theta_j}h_j' = \tilde{z}_j \\ Re^{i\theta_j}h_j'' = -2\beta u_0 u_0^* - \dfrac{1}{N}\displaystyle\sum_{\substack{l=1 \\ l\neq j}}^{N} \nabla W(\tilde{y}_j - \tilde{y}_l) \end{cases} \quad , \quad j = 1, \dots, N.$$

From the previous equation, we can characterize h_j'' as

$$h_j'' = \sum_{l\neq j}\Big[G_1(\phi/2)(h_j - e^{i\phi}h_l) + G_2(\phi/2)(\bar{h_l} - e^{i\phi}\bar{h_j})]\Big] - 2\beta u_0 u_0^T h_j',$$

where $\phi = \frac{2\pi(l-j)}{N}$ and

$$\begin{aligned} G_1(\phi) =& \frac{1}{2N}\left[-a(2R|\sin\phi|)^{a-2} + b(2R|\sin\phi|)^{b-2}\right], \\ G_2(\phi) =& \frac{1}{2N}\left[-(a-2)(2R|\sin\phi|)^{a-2} + (b-2)(2R|\sin\phi|)^{b-2}\right], \end{aligned}$$

for the power law potentials. The details of these previous computations for general potentials can be found in [6].

Let us consider the following ansatz for perturbations h_j

$$h_j = \xi_+(t)e^{im\theta_j} + \xi_-(t)e^{-im\theta_j}, \qquad m = 2, 3, \dots, \tag{13}$$

which satisfies conditions (12). We need to exclude the case $m = 1$ since it leads to a zero eigenvalue due to the rotational invariance of the system. Following the same strategy as in [6] and some computations, we finally deduce

$$\begin{pmatrix} \xi_+'' \\ \xi_-'' \end{pmatrix} = \underbrace{\begin{pmatrix} I_1(m) & I_2(m) \\ I_2(m) & I_1(-m) \end{pmatrix}}_{M} \begin{pmatrix} \xi_+ \\ \xi_- \end{pmatrix} - 2\beta u_0 u_0^T \begin{pmatrix} \xi_+' \\ \xi_-' \end{pmatrix},$$

with I_1 and I_2 real functions given by

$$I_1(m) = \sum_{l\neq j} G_1(\phi/2)(1 - e^{i(m+1)\phi}) = 4\sum_{p=1}^{N/2} G_1\left(\frac{\pi p}{N}\right)\sin^2\left(\frac{(m+1)\pi p}{N}\right), \tag{14}$$

$$I_2(m) = \sum_{l\neq j} G_2\left(\phi/2\right)\left(e^{im\phi} - e^{i\phi}\right) = 4\sum_{p=1}^{N/2} G_2\left(\frac{\pi p}{N}\right)\left[\sin^2\left(\frac{\pi p}{N}\right) - \sin^2\Big(\frac{m\pi p}{N}\Big)\right]. \tag{15}$$

The previous system can be written also in the following form

$$\frac{d}{dt}\begin{pmatrix} \xi_+ \\ \bar{\xi_-} \\ \eta_+ \\ \bar{\eta_-} \end{pmatrix} = \begin{pmatrix} 0 & \mathrm{Id} \\ M & -2\beta u_0 u_0^T \end{pmatrix}\begin{pmatrix} \xi_+ \\ \xi_- \\ \eta_+ \\ \eta_- \end{pmatrix} = L\begin{pmatrix} \xi_+ \\ \xi_- \\ \eta_+ \\ \eta_- \end{pmatrix}, \tag{16}$$

where $(\eta_+, \eta_-) = (\xi_+', \xi_-')$.

If we do not assume (12) and (13), then we cannot reduce the analysis to a 4×4 system. An arbitrary perturbation for general flocks leads instead to a matrix of the form

$$L = \begin{pmatrix} 0 & \mathrm{Id} \\ \mathbf{M} & -2\beta U \end{pmatrix},$$

where the partition into $2N \times 2N$ sub-blocks reflects the distinction between position and velocity contributions to the Jacobian: The symmetric matrix $\mathbf{M}$ is the $2N \times 2N$ Hessian that results from linearizing the first order system (2) about a given flocking configuration, whereas U denotes a block-diagonal matrix with N blocks of the 2×2 matrix $u_0 u_0^T$ along the diagonal. By rotational invariance we can reduce to the case $u_0 = e_1 = (1, 0)$, so that the block matrix U acts on $\mathbf{x} = (x_1, \ldots, x_N)^T \in \mathbb{R}^{2N}$, $x_i \in \mathbb{R}^2$, according to the relation

$$(U\mathbf{x})_i = \begin{pmatrix} \langle x_i, e_1 \rangle \\ 0 \end{pmatrix}.$$

We now turn to the task of characterizing the eigenvalues of L in terms of the eigenvalues of $\mathbf{M}$. In other words, we aim to characterize the stability of a flock in terms of the stability of its spatial shape as a solution to the first order model. To fix the notation, we write the eigenvalue problem for the flock as

$$\lambda \begin{pmatrix} \mathbf{x} \\ \mathbf{v} \end{pmatrix} = \begin{pmatrix} 0 & \mathrm{Id} \\ \mathbf{M} & -2\beta U \end{pmatrix} \begin{pmatrix} \mathbf{x} \\ \mathbf{v} \end{pmatrix} = L \begin{pmatrix} \mathbf{x} \\ \mathbf{v} \end{pmatrix}, \tag{17}$$

where the matrix $\mathbf{M}$ determines the stability of the flocking configuration as a solution of the first order model. For any given eigenvector $(\mathbf{x}, \mathbf{v}) \in \mathbb{C}^{2N} \times \mathbb{C}^{2N}$ of the full system (17), we always assume the normalization $\mathbf{x}^*\mathbf{x} = 1$. Substituting the first equation $\lambda \mathbf{x} = \mathbf{v}$ into the second equation yields the equivalent statement

$$\lambda^2 \mathbf{x} + 2\beta\lambda U\mathbf{x} - \mathbf{M}\mathbf{x} = 0. \tag{18}$$

Let $|\mathbf{x}|_2$ denote the semi-norm on $\mathbb{C}^{2N}$ defined according to

$$|\mathbf{x}|_2^2 := \sum_{i=1}^{N} |\langle x_i, e_1 \rangle|^2,$$

and let $E^N \cong \mathbb{C}^N$ denote the subspace

$$E^N := \left\{ \mathbf{x} \in \mathbb{C}^{2N} : |\mathbf{x}|_2 = 0 \right\} = \ker(U).$$

Premultiplying by $\mathbf{x}^*$, the fact that $\mathbf{x}^* U \mathbf{x} = |\mathbf{x}|_2^2$, the normalization on $\mathbf{x}$ and the quadratic formula combine to imply the key identity

$$\lambda = -\beta |\mathbf{x}|_2^2 \pm \sqrt{\beta^2 |\mathbf{x}|_2^4 + \mathbf{x}^* \mathbf{M} \mathbf{x}}. \tag{19}$$

As $\mathbf{M}$ is symmetric, we may write its $2N$ real eigenvalues and corresponding normalized ($\mathbf{x}^*\mathbf{x} = 1$) eigenvectors as

$$\mu_{2N} \leqslant \mu_{2N-1} \leqslant \cdots \leqslant \mu_2 \leqslant \mu_1 \qquad \mathbf{M}\mathbf{x}_i = \mu_i \mathbf{x}_i.$$

The notation $a_L(\lambda)$, $a_{\mathbf{M}}(\mu)$ will denote the algebraic multiplicities of λ, μ as eigenvalues of their respective matrices. The bulk of the analysis lies in characterizing the eigenvalues λ of the full system (17) that have $\Re(\lambda) = 0$.

Lemma 2. *Let λ denote an eigenvalue of (17). Then $\Re(\lambda) = 0$ and $\Im(\lambda) \neq 0$ if and only if $\lambda = \pm i\sqrt{-\mu_k}$ for some k with $\mu_k < 0$ and $\mathbf{x}_k \in E^N$. The eigenspace consists only of eigenvectors.*

Proof. If $\mathbf{x}_k \in E^N$ then (18) reads $\lambda^2 \mathbf{x}_k = \mathbf{M}\mathbf{x}_k$, or equivalently $\lambda^2 = \mu_k$. To have $\Im(\lambda) \neq 0$ then requires $\mu_k < 0$. Conversely, if $(\mathbf{x}, \lambda\mathbf{x})$ denotes an eigenvector with $\Re(\lambda) = 0$ and $\Im(\lambda) \neq 0$, the formula (19) implies that necessarily $\mathbf{x} \in E^N$, and therefore $\mathbf{M}\mathbf{x} = \lambda^2\mathbf{x}$. Thus $\lambda^2 = \mu_k$ for some $\mu_k < 0$.

To show the last statement, suppose a generalized eigenvector existed that is not an eigenvector. Then there exists an eigenvector $(\mathbf{x}, \lambda\mathbf{x})$ with $\mathbf{x} \in E^N$ so that the system of equations

$$\begin{pmatrix} -\lambda \mathrm{Id} & \mathrm{Id} \\ \mathbf{M} & -2\beta U - \lambda \mathrm{Id} \end{pmatrix} \begin{pmatrix} \mathbf{u} \\ \mathbf{w} \end{pmatrix} = \begin{pmatrix} \mathbf{x} \\ \lambda \mathbf{x} \end{pmatrix} \tag{20}$$

has a non-trivial solution. Substituting the first equation $\mathbf{w} = \lambda\mathbf{u} + \mathbf{x}$ into the second equation, then pre-multiplying by $\mathbf{x}^*$ demonstrates

$$\mathbf{M}\mathbf{u} - 2\beta U \mathbf{w} = 2\lambda \mathbf{x} + \lambda^2 \mathbf{u}$$
$$\mathbf{x}^* \mathbf{M}\mathbf{u} = 2\lambda + \lambda^2 \mathbf{x}^* \mathbf{u}.$$

The last line follows as $\mathbf{x}^*\mathbf{x} = 1$ and $\mathbf{x} \in E^N = \ker(U)$. The symmetry of $\mathbf{M}$ and the fact that $\mathbf{M}\mathbf{x} = \lambda^2\mathbf{x}$ combine to show $\mathbf{x}^*\mathbf{M}\mathbf{u} = \lambda^2 \mathbf{x}^*\mathbf{u}$. Thus $\lambda = 0$, leading to a contradiction. □

Lemma 3. *Let $\beta > 0$. Then $\lambda = 0$ is an eigenvalue of (17) and $(\mathbf{x}, \mathbf{0})$ is a corresponding eigenvector if and only if $\mathbf{M}\mathbf{x} = \mathbf{0}$. If $\mathbf{x} \in E^N$ then $(\mathbf{x}, \mathbf{0})$ generates a single generalized eigenvector, whereas if $\mathbf{x} \notin E^N$ then $(\mathbf{x}, \mathbf{0})$ generates no generalized eigenvectors.*

Proof. The first statement follows trivially from (18). To see the second statement, consider the system of equations (20) with $\lambda = 0$. This reduces to the equations $\mathbf{w} = \mathbf{x}$ and

$$\mathbf{M}\mathbf{u} = 2\beta U \mathbf{x},$$

which by premultiplying by $\mathbf{x}^*$ as before and using the fact that $\mathbf{M}\mathbf{x} = \mathbf{0}$ necessitates $\mathbf{x} \in E^N$ as $\beta > 0$. If indeed $\mathbf{x} \in E^N$ then any $\mathbf{u} \in \ker(\mathbf{M})$ suffices. Without loss of generality, take $\mathbf{u} = \mathbf{x}$ itself. If $(\mathbf{x}, \mathbf{0})$ generates a second generalized eigenvector then the system of equations

$$\begin{pmatrix} 0 & \mathrm{Id} \\ \mathbf{M} & -2\beta U \end{pmatrix} \begin{pmatrix} \mathbf{u} \\ \mathbf{w} \end{pmatrix} = \begin{pmatrix} \mathbf{x} \\ \mathbf{x} \end{pmatrix}$$

has a non-trivial solution. As then $\mathbf{w} = \mathbf{x}$ and $\mathbf{x} \in E^N$ this reads $\mathbf{M}\mathbf{u} = \mathbf{x}$. Premultiplying one last time by $\mathbf{x}$, the facts that $\mathbf{M}\mathbf{x} = \mathbf{0}$ and $\mathbf{x}^*\mathbf{x} = 1$ combine to produce the contradiction $0 = 1$. □

This lemma yields, as a corollary, the algebraic multiplicity $a_L(0)$ of zero as an eigenvalue of the second order system.

Corrolary 1. *Let $\beta > 0$. Then*

$$a_L(0) = \dim(\ker(\mathbf{M}) \cap E^N) + \dim(\ker(\mathbf{M})).$$

Let $a_{\mathbf{M},\perp}(0) := \dim(\ker(\mathbf{M}) \cap E^N)$, so that $a_L(0) = a_{\mathbf{M},\perp}(0) + a_{\mathbf{M}}(0)$. Note that neither quantity depends on β, and the conclusion holds whenever β is positive. Thus, if $\beta \in (0, \infty)$ it follows that $a_L(0)$ is constant. Moreover, Lemma 2 holds uniformly in β as well. Let $i_1 < i_2 < \cdots < i_k \leqslant 2N$ denote those (possibly non-existent) indices where $\mu_{i_j} < 0$ has an eigenvector $\mathbf{x}_{i_j} \in E^N$. The two lemmas then combine to show:

Corrolary 2. *Let $\beta > 0$. Then*

$$\det(L - \lambda \mathrm{Id}) = \lambda^{a_{\mathbf{M},\perp}(0)+a_{\mathbf{M}}(0)} \Pi_{j=1}^{k} (\lambda^2 - \mu_{i_j}) p_\beta(\lambda).$$

The roots of the polynomial $p_\beta(\lambda)$ all have non-zero real part.

This corollary, along with the formula (19), suffice to establish the desired result:

Theorem 1. *The linearized second order system around the flock ring solution* (1) *has an eigenvalue with positive real part if and only if the linearized first order system around the ring solution has a positive eigenvalue. As a consequence, the flock ring solution is unstable for m-mode perturbations for the second order model* (1) *if and only if the ring solution is unstable for m-mode perturbations for the first order model* (2)*.*

Proof. Suppose first that $\mu_1 \leqslant 0$. Then $\mathbf{x}^* \mathbf{M} \mathbf{x} \leqslant 0$ for any $\mathbf{x}$, whence all eigenvalues λ of L have non-positive real part due to (19). Conversely, suppose $\mu_1 > 0$ and let $\mathcal{A}$ denote the set

$$\mathcal{A} := \left\{ \beta \in [0, \infty) : \max_{\lambda \in \sigma(L)} \Re(\lambda) > 0 \right\}.$$

Note that $0 \in \mathcal{A}$ due to (19). Indeed, then $(\mathbf{x}_1, \sqrt{\mu_1}\mathbf{x}_1)$ defines an eigenvector with eigenvalue $\lambda = \sqrt{\mu_1} > 0$. By continuous dependence of the eigenvalues of L on β, it follows that $\mathcal{A}$ is relatively open. To show that it is also relatively closed, let $\beta_l \in \mathcal{A}$ and $\beta_l \to \beta_0 \in (0, \infty)$. Up to extraction of subsequences, it follows that there exists a corresponding sequence λ_l of eigenvalues with $\Re(\lambda_l) > 0$ converging to some λ_0 with $\Re(\lambda_0) \geqslant 0$. Moreover, by continuous dependence of the coefficients of $p_\beta(\lambda)$ on β, the roots of $p_{\beta_l}(\lambda)$ converge to roots of $p_{\beta_0}(\lambda)$. Thus $p_{\beta_0}(\lambda_0) = 0$. As no such root can have zero real part by corollary 2, $\Re(\lambda_0) > 0$ and $\beta_0 \in \mathcal{A}$. As $\mathcal{A} \neq \varnothing$ it follows that $\mathcal{A} = [0, \infty)$ as desired. The last part of the theorem is a direct application of the first part to the $4x4$ m-mode perturbation matrix in (16). □

Remark 4. *As an artifact of translation invariance in the first order model, the vector defined by $\mathbf{e}_2 := (0, 1, \ldots, 0, 1)^T \in \mathbb{R}^{2N}$ always defines an eigenvector of $\mathbf{M}$ with eigenvalue zero. Due to the fact that $\mathbf{e}_2 \in E^N$, Lemma 3 implies that $(\mathbf{e}_2, \mathbf{e}_2)$ furnishes a generalized eigenvector with eigenvalue zero, so that the flock is always linearly unstable for the model* (1)*.*

3.2. **Numerical validations.** In this section, we perform some numerical computations to show stability regions for the flock ring. Moreover, we will show the formation of clusters and the fattening instability. Due to Theorem 1 and Corollary 4, applied to the 4×4 matrix in (16), we are reduced to study the determinant of the matrix M for the flock stability. Note that for fixed values of N and m the determinant of M is a function of the parameters a and b and such that

$$D(a, b) := \det(M) = I_1(m) I_1(-m) - (I_2(m))^2,$$
$$T(a, b) := \mathrm{trace}(M) = I_1(m) + I_1(-m).$$

Remark 5. *Using the results of* [6, Theorem 3.1] *one is able to estimate the asymptotic value of the determinant of M. In our case, using $W(x) = \frac{|x|^a}{a} - \frac{|x|^b}{b}$ one obtains that*

$$\det(M) \sim C m^{-b+1} \quad as \quad m \to \infty,$$

where $C > 0$ and $b \in (1, 2) \cup (4, 6) \cup (8, 10) \cup \cdots$. In these cases $\det(M) > 0$ and $\mathrm{trace}(M) < 0$. Moreover, this result shows that there is no spectral gap for large modes m since $\det(M) \to 0$ as $m \to \infty$.

In Figure 2 we recover some results on the stability already shown in [25] . Since $I_1(m)$ and $I_2(m)$ depend on the powers a and b of the power law potential, we plot in the parameter region $\{(a,b) : a > b > 0\}$ the stability and instability regions depending on the determinant of M and its trace. We show the cases $m = 3, 4, 5$ for a fixed $N = 100000$. In Figure 3 we

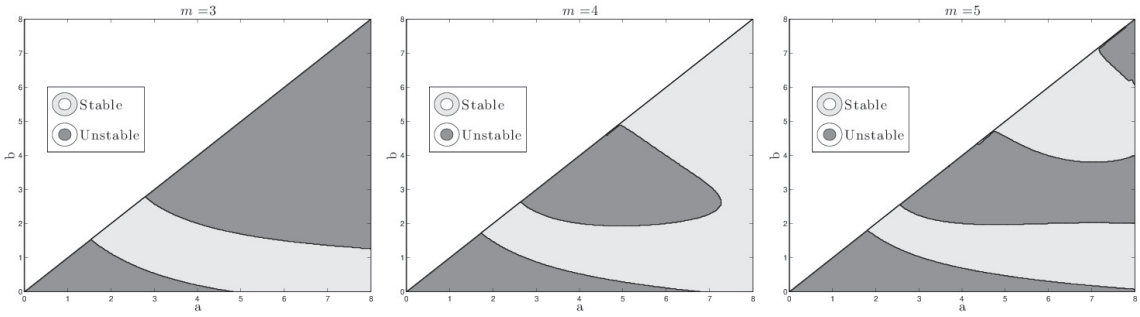

FIGURE 2. Stability regions for different perturbations modes $m = 3, 4, 5$. Stability regions correspond to a couple (a, b) of parameters where $D(a, b) > 0, \quad T(a, b) < 0$.

compute the stability area as a function of a and b. To do so, we compute the intersection of all stability areas for $m \geqslant 2$. It can be observed from our tests that the stability area shrinks when the number of particles increases. Moreover, it is observed that in the limit when $N \to \infty$, the lower boundary of the stability region converges to the dashed line. The red dashed line is the curve $b = \frac{a}{a-1}$ that corresponds to the $m = +\infty$ mode. This curve is the separatrix of the ins/stability regions for the continuous delta ring of the first order continuum model, studied in [25, 3].

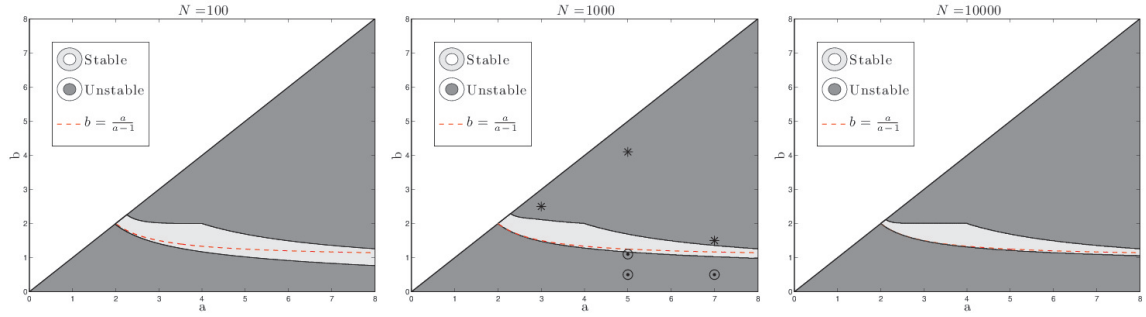

FIGURE 3. Stability areas for flock ring solutions for different values of N. From left to right: $N = 100, 1000, 10000$. Markers $(\ast)$ and $(\odot)$ indicate the explored parameters respectively in Table 1 and Table 2.

3.2.1. *Cluster formation.* The formation of clusters occurs when the repulsion strength is small. In other words, this phenomenon depends on how singular the potential is at the origin. We show the bifurcation diagram for the phase transition between equally distributed flock and flock with cluster formation. Figure 4 is performed using $N = 1000$ particles equally distributed on the stable circle with all the velocities aligned. We let them evolve

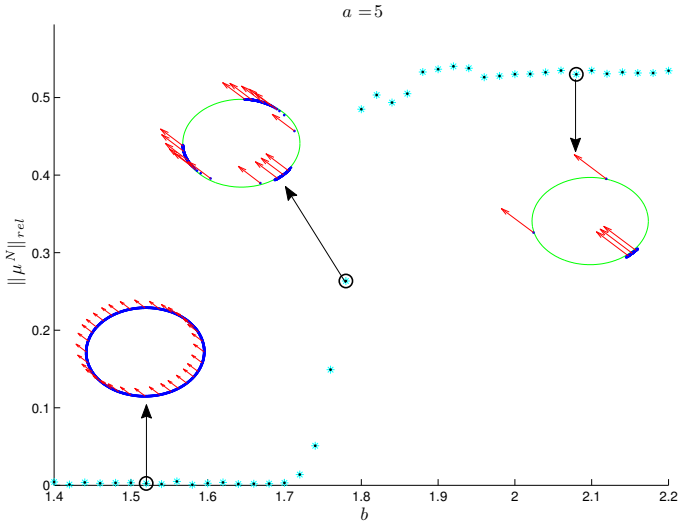

FIGURE 4. Bifurcation diagram for cluster formation at $T_f = 500$, with $N = 1000$ particles, $a = 5$, $|u_0| = 2.5$.

until $T_f = 500$. We fix the parameters $|u_0| = 2.5$, $a = 5$ and vary b along the axis. The vertical axis represents the increment of the relative errors

$$\|\mu^N\|_{rel} = \frac{\|\mu^N - \mu_0^N\|_2}{\|\mu_0^N\|_2}$$

with increasing b, where μ_0^N is the uniform distribution along the stable ring of N particles and μ^N the distribution at time T_f. Simulations are performed with *MATLAB* and the evolution of the system of odes is solved with the *ode45* routine with adaptive time step. Table 1 illustrates different possible final states for different choices of the parameters a, b.

$a = 3, b = 2.5$	$a = 5, b = 4.1$	$a = 7, b = 1.5$
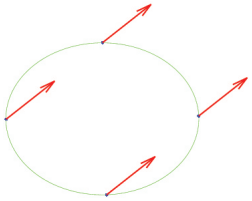	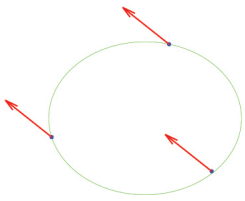	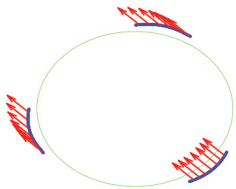

TABLE 1. Long time simulations with $N = 1000$ particles. The location of parameter values are marked as $(*)$ points in the central plot of Figure 3.

3.2.2. *Fattening formation.* We show the transition diagram between a flock on a ring and a flock on an annulus. In this case, the fattening phenomenon occurs when the parameters of the potential cross the lower boundary of the stability region. We numerically characterize this behavior in a similar way as in the previous subsection.

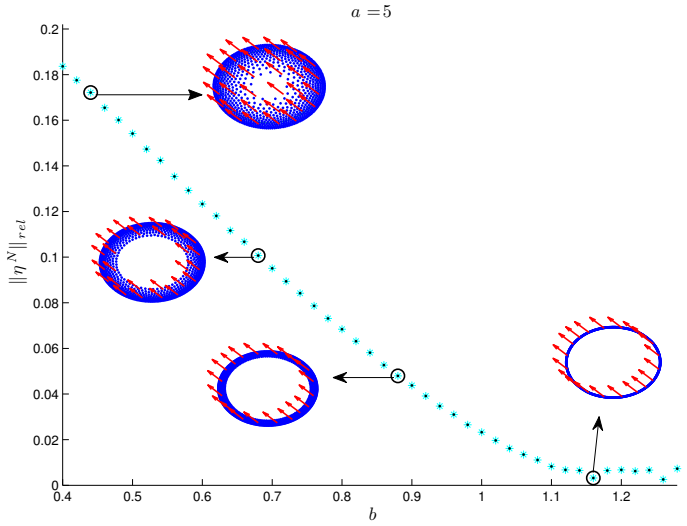

FIGURE 5. Bifurcation diagram for fattening instability at $T_f = 500$ with N=1000 particles, $a = 5$, $|u_0| = 2.5$.

Figure 5 is performed using $N = 1000$ particles equally distributed on the stable ring already in the steady state with all the velocities aligned. We then let them evolve until $T_f = 500$. We fix the parameters $|u_0| = 2.5$, $a = 5$ and vary b along the axis. The vertical axis represents the increment of the relative errors

$$\|\eta^N\|_{rel} = \frac{\|\eta^N - \eta_0^N\|_2}{\|\eta_0^N\|_2}$$

for increasing b, where η_0^N represents the average distance from the center of mass for N particles in a flock ring formation, i.e., $\eta_0^N = R$ and η^N is the average distance from the center of mass at time T_f. Table 2 shows the final states for some particular choices of parameters after stabilization.

$a = 5, b = 1.1$	$a = 5, b = 0.5$	$a = 7, b = 0.5$
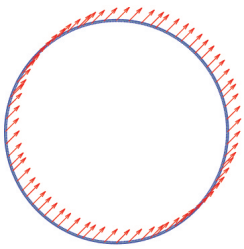	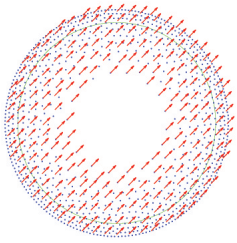	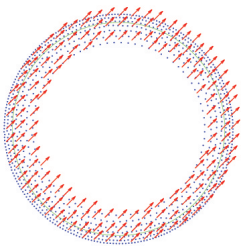

TABLE 2. Long time simulations with $N = 1000$ particles. The location of parameter values are marked as ($\odot$) points in the central plot of Figure 3.

3.3. **Stability of flock solutions with the Cucker-Smale alignment term.** As in Section 3.1 we perform a study on the flock stability for model (3). If we use the same change of variables as in (11), then system (3) reads

$$\begin{cases} \dot{y}_j = v_j - u_0 = z_j \\ \dot{z}_j = \dfrac{1}{N}\displaystyle\sum_{l=1}^{N} H(|y_l - y_j|)(z_l - z_j) + \dfrac{1}{N}\sum_{\substack{l=1 \\ l\neq j}}^{N} \nabla W(y_l - y_j) \end{cases}, \qquad j = 1, \dots, N \tag{21}$$

We give a characterization of the flock solution in the complex plane for (21) with $(y_j^0, z_j^0) = (Re^{i\theta_j}, 0)$, where $\theta_j = \frac{2\pi j}{N}$. We consider then the perturbed solution

$$\tilde{y}_j(t) = Re^{i\theta_j}(1 + h_j(t)),$$

with h_j such that $|h_j| \ll 1$ and satisfying (12). Considering the following relations

$$\begin{aligned} &\tilde{y}_l - \tilde{y}_j = Re^{i\theta_j}\left(e^{\phi_p} h_l - h_j\right), \\ &|\tilde{y}_l - \tilde{y}_j| \simeq 2R\left|\sin\left(\frac{\phi_p}{2}\right)\right| + \frac{R}{4\left|\sin\left(\frac{\phi_p}{2}\right)\right|}\left[\left(1 - e^{i\phi_p}\right)\left(h_l - \overline{h_j}\right) + \left(1 - e^{-i\phi_p}\right)\left(\overline{h_l} - h_j\right)\right], \\ &\tilde{z}_l - \tilde{z}_j = Re^{i\theta_j}\left(e^{\phi_p} h_l' - h_j'\right), \end{aligned}$$

where $\phi_p = 2\pi(l-j)/N = 2\pi p/N$. We linearize the Cucker-Smale alignment term around the solution up to first order, leading to

$$\begin{aligned} H(|\tilde{y}_l - \tilde{y}_j|) \simeq & H(2R\,|\sin(\phi_p/2)|) \\ & + H'(2R\,|\sin(\phi_p/2)|)\frac{R}{4\left|\sin\left(\frac{\phi_p}{2}\right)\right|}\left[\left(1 - e^{i\phi_p}\right)\left(h_l - \overline{h_j}\right) + \left(1 - e^{-i\phi_p}\right)\left(\overline{h_l} - h_j\right)\right]. \end{aligned}$$

Substituting the linearization in (21) and neglecting the second order terms, we obtain the following characterization of h_j''

$$\begin{aligned} h_j'' = & \frac{1}{N}\sum_{l=1}^{N} H(2R|\sin\phi_p|)\left[e^{i\phi_p} h_l' - h_j'\right] \\ & + \frac{1}{N}\sum_{\substack{l=1 \\ l\neq j}}^{N}\left[G_1(\phi_p/2)(h_j - e^{i\phi_p} h_l) + G_2(\phi_p/2)(\overline{h_l} - e^{i\phi_p}\overline{h_j})\right]. \end{aligned} \tag{22}$$

In order to study the behavior of the perturbations h_j, we reduce the complexity of the problem, assuming that h_j satisfies the following relation

$$h_j = \xi_+(t)e^{im\theta_j} + \xi_-(t)e^{-im\theta_j}, \quad h_j' = \xi_+'(t)e^{im\theta_j} + \xi_-'(t)e^{-im\theta_j}, \qquad m \in \mathbb{N}.$$

Therefore, we can express h_l in terms of h_j as

$$h_l = \xi_+(t)e^{im\theta_j}e^{im\phi_p} + \xi_-(t)e^{-im\theta_j}e^{-im\phi_p}, \qquad m \in \mathbb{N}.$$

Inserting the previous expressions in (22) and gathering terms in $e^{i\theta_j m}$ and $e^{-i\theta_j m}$, we can characterize ξ_+ and ξ_- as

$$\begin{aligned}\xi_+'' =&\frac{1}{N}\sum_{l=1}^{N} H(2R|\sin\phi_p|)\left[e^{i\phi_p(m+1)}-1\right]\xi_+' + I_1(m)\xi_+ + I_2(m)\overline{\xi}_-,\\ \overline{\xi}_-'' =&\frac{1}{N}\sum_{l=1}^{N} H(2R|\sin\phi_p|)\left[e^{i\phi_p(m-1)}-1\right]\overline{\xi}_- + I_2(m)\xi_+ + I_1(-m)\overline{\xi}_-,\end{aligned}$$

where I_1 and I_2 are defined in (14) and (15). Through a simple manipulation of the sum for the linearized *Cucker-Smale* term, we obtain that the expression

$$\begin{aligned}&\frac{1}{N}\sum_{l\neq j} H(2R|\sin\phi_p|)\left[e^{i\phi_p(m\pm1)}-1\right] =\\ &\qquad\frac{1}{N}\sum_{l\neq j} H(2R|\sin\phi_p|)\left[\cos(\phi_p(m\pm1))-1\right] + \frac{i}{N}\sum_{l\neq j} H(2R|\sin\phi_p|)\sin(\phi_p(m\pm1)),\end{aligned}$$

is real. Actually, $H(2R|\sin\phi_p|)$ and $\sin(\phi_p(m\pm1))$ are respectively symmetric and anti-symmetric with respect to the values of ϕ_p, so the imaginary part vanishes. Recalling the definition of ϕ_p, we conclude

$$\begin{aligned}J_\pm(m) =&\frac{1}{N}\sum_{k=1}^{N} H\left(2R\left|\sin\left(\frac{2\pi p}{N}\right)\right|\right)\left[\cos\left(\frac{2\pi p}{N}(m\pm1)\right)-1\right]\\ =&-\frac{4}{N}\sum_{k=1}^{N/2} H\left(2R\left|\sin\left(\frac{2\pi p}{N}\right)\right|\right)\left[\sin^2\left(\frac{\pi p}{N}(m\pm1)\right)\right].\end{aligned}$$

Therefore, we reduce the stability analysis to the following system

$$\begin{pmatrix}\xi_+''\\ \overline{\xi}_-''\end{pmatrix} = \underbrace{\begin{pmatrix}I_1(m) & I_2(m)\\ I_2(m) & I_1(-m)\end{pmatrix}}_{M}\begin{pmatrix}\xi_+\\ \overline{\xi}_-\end{pmatrix} + \underbrace{\begin{pmatrix}J_+(m) & 0\\ 0 & J_-(m)\end{pmatrix}}_{J}\begin{pmatrix}\xi_+'\\ \overline{\xi}_-'\end{pmatrix}.$$

Taking the conjugate in the second equation and relabeling $\overline{\xi}_-$ with ξ_- as in [6], the previous system is equivalent to

$$\frac{d}{dt}\begin{pmatrix}\xi_+\\ \xi_-\\ \eta_+\\ \eta_-\end{pmatrix} = \begin{pmatrix}0 & 0 & 1 & 0\\ 0 & 0 & 0 & 1\\ I_1(m) & I_2(m) & J_+(m) & 0\\ I_2(m) & I_1(-m) & 0 & J_-(m)\end{pmatrix}\begin{pmatrix}\xi_+\\ \xi_-\\ \eta_+\\ \eta_-\end{pmatrix} = \begin{pmatrix}0 & \mathrm{Id}\\ M & J\end{pmatrix}\begin{pmatrix}\xi_+\\ \xi_-\\ \eta_+\\ \eta_-\end{pmatrix}, \tag{23}$$

where $\eta_\pm = \xi_\pm'$.

At this point, we will do a stability analysis based on the eigenvalues of the matrix of the previous system in a similar way as in Section 3.1. If instead of the self-propelled/ friction term we use a Cucker-Smale type alignment term

$$-\sum_{l=1}^{N} g\left(|x_j - x_l|\right)(v_j - v_l),$$

where $g(r)$ denotes any strictly positive function, the corresponding stability matrix L_{CS} for the flock reads

$$L_{\text{CS}} = \begin{pmatrix} 0 & \text{Id} \\ \mathbf{M} & -G \end{pmatrix}.$$

As before, $\mathbf{M}$ denotes stability matrix of the first order model. As the alignment term is linear in the velocity, the matrix G acts on $\mathbf{v} = (v_1, \dots, v_N)^T$, $v_j \in \mathbb{R}^2$, according to the relation

$$(G\mathbf{v})_j = \sum_{l=1}^{N} g\left(|x_j - x_l|\right)(v_j - v_l).$$

In particular, if we denote $||v_j - v_l||_2^2 := (v_j - v_l)^*(v_j - v_l)$ then this relation implies that

$$\mathbf{v}^* G\mathbf{v} = \frac{1}{2} \sum_{j,l=1}^{N} g\left(|x_j - x_l|\right) ||v_j - v_l||_2^2.$$

Consequently, G is positive semi-definite and $G\mathbf{v} = \mathbf{0}$ if and only if $\mathbf{v}$ is "constant" in the sense that $v_j \equiv w$ for some fixed $w \in \mathbb{R}^2$. In other words, $\ker(G) = \text{span}\{\mathbf{e}_1, \mathbf{e}_2\}$. By translation invariance of the first order model, both $\mathbf{e}_1 \in \ker(\mathbf{M})$ and $\mathbf{e}_2 \in \ker(\mathbf{M})$ as well.

Note that the eigenvalue problem for L_{CS} is again equivalent to the following quadratic eigenvalue problem for $\mathbf{x} \in \mathbb{C}^{2N}$: $\lambda^2\mathbf{x} + \lambda G\mathbf{x} - \mathbf{M}\mathbf{x} = \mathbf{0}$. Assuming the normalization $\mathbf{x}^*\mathbf{x} = 1$, the quadratic formula then implies that

$$\lambda = \frac{-\mathbf{x}^* G\mathbf{x} \pm \sqrt{(\mathbf{x}^* G\mathbf{x})^2 + 4\mathbf{x}^*\mathbf{M}\mathbf{x}}}{2}.$$

From this relation and the fact that $\ker(G) \subset \ker(\mathbf{M})$ we conclude that $\ker(L_{\text{CS}}) = \ker(\mathbf{M})$, and moreover that $\Re(\lambda) = 0 \quad \Leftrightarrow \quad \lambda = 0$. Furthermore, $\mathbf{e}_1$ and $\mathbf{e}_2$ generate a single generalized eigenvector whereas each remaining $\mathbf{x} \in \ker(\mathbf{M})$ generates no generalized eigenvectors. Indeed, corresponding to each $\mathbf{x} \in \ker(\mathbf{M})$ the system of equations

$$\begin{pmatrix} 0 & \text{Id} \\ \mathbf{M} & -G \end{pmatrix} \begin{pmatrix} \mathbf{u} \\ \mathbf{w} \end{pmatrix} = \begin{pmatrix} \mathbf{x} \\ \mathbf{0} \end{pmatrix}.$$

has a solution if and only if $G\mathbf{x} = \mathbf{0}$ and $\mathbf{u} \in \ker(\mathbf{M})$. Additionally, if $\mathbf{x} = \mathbf{e}_i$ then for any $\mathbf{u} \in \ker(\mathbf{M})$ the system of equations

$$\begin{pmatrix} 0 & \text{Id} \\ \mathbf{M} & -G \end{pmatrix} \begin{pmatrix} \tilde{\mathbf{u}} \\ \tilde{\mathbf{w}} \end{pmatrix} = \begin{pmatrix} \mathbf{u} \\ \mathbf{x} \end{pmatrix}$$

has no solutions. This follows by multiplying the second equation by $\mathbf{x}^*$, then using the facts that $\mathbf{e}_i \in \ker(G) \subset \ker(\mathbf{M})$ and the facts that G and $\mathbf{M}$ are symmetric. In other words, if $g(r)$ is any strictly positive function then

$$\det(L_{\text{CS}} - \lambda\text{Id}) = \lambda^{2+\dim(\ker(\mathbf{M}))} p_g(\lambda),$$

for some polynomial $p_g(\lambda)$ that has non-zero roots. Since this equation holds for any strictly positive function $g(r)$, we may follow the proof of Theorem 1 to conclude that the second order model has an eigenvalue with positive real part if and only if the first order system has a positive eigenvalue. Moreover, the vectors $(\mathbf{e}_i, \mathbf{e}_i)$ for each $i = 1, 2$ furnish generalized eigenvectors with eigenvalue zero, so the ring flock is always linearly unstable. As a summary, we have shown:

Theorem 2. *The linearized second order system* (3) *around the flock ring solution has an eigenvalue with positive real part if and only if the linearized first order system around the ring solution has a positive eigenvalue. As a consequence, the flock ring solution is unstable for m-mode perturbations for the second order model* (3) *if and only if the ring solution is unstable for m-mode perturbations for the first order model* (2).

The linear stability analysis of the previous system leads to the characterization of the stability areas in Figure 6. We show that the stability parameter regions for different values of N, and $\gamma = 1$ coincide with the ones in Figure 3.

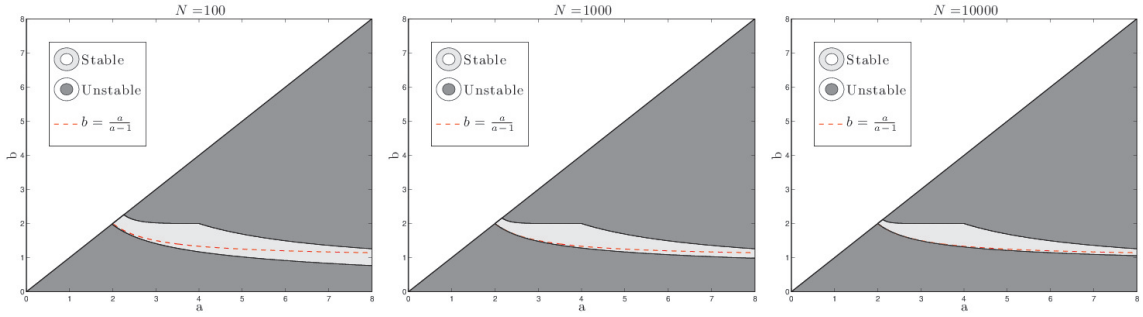

FIGURE 6. Stability regions for flock ring solutions with the Cucker-Smale term for different values of N.

We also investigate the behavior of the eigenvalue with the largest real part, $\Re(\lambda_1)$, of the linearized system (23) against the increasing value of communication strength γ. In Figure 7, as the potential gets more repulsive at the origin, we see the change from stability to instability, and the rate of convergence to equilibrium depending on γ.

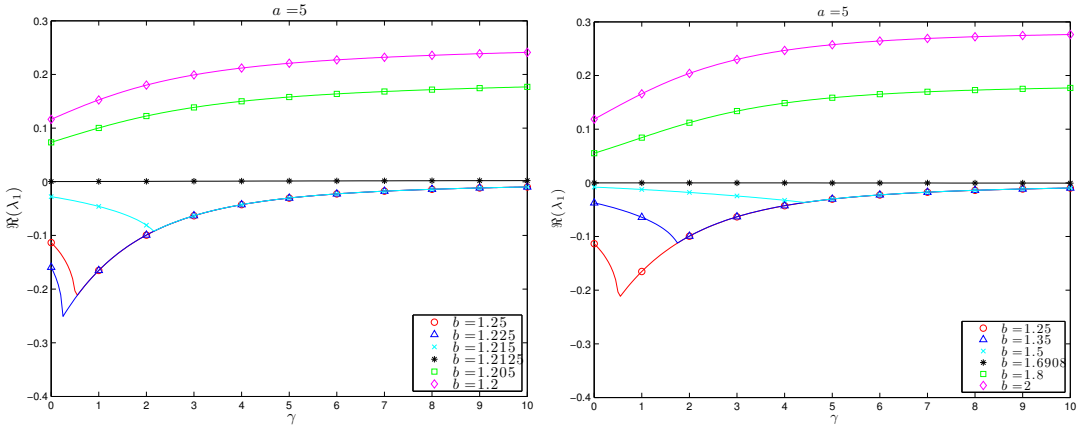

FIGURE 7. The magnitude of $\Re(\lambda_1)$ is influenced by γ, for different values of b and fixed $a = 5$, $N = 10000$.

4. Stability for mill solutions

This section is devoted to complement the results in [6] by analyzing the stability of mill ring solutions with repulsion.

4.1. **Linear stability analysis.** Let us consider the transformation

$$\begin{cases} y_j(t) = O(t)x_j(t) \\ z_j(t) = O(t)v_j(t) \end{cases} \quad , \quad j = 1, \dots, N$$

where $O(t)$ is the rotation matrix defined as

$$O(t) = e^{St}, \quad S = \begin{pmatrix} 0 & \omega \\ -\omega & 0 \end{pmatrix}, \quad \text{and} \quad \dot{O}(t) = Se^{St}.$$

Evaluating $\dot{y}_j(t)$ and $\dot{z}_j(t)$ and after some straightforward computations, we get

$$\begin{cases} \dot{y}_j(t) = Sy_j(t) + z_j(t) \\ \dot{z}_j(t) = Sz_j(t) + (\alpha - \beta|z_j|^2)z_j(t) - \dfrac{1}{N}\displaystyle\sum_{\substack{l=1 \\ l\neq j}}^{N} \nabla W(y_l - y_j) \end{cases} \quad , \quad j = 1, \dots, N.$$

A linear stability analysis for mill rings was performed in [6]. Actually, for a fixed number of particles, we have a mill ring solution given by $(y_j^0, z_j^0) = (Re^{i\theta_j}, 0)$, where $\theta_j = \frac{2\pi j}{N}$, and R determined by equation (7). With the same notation as in Section 3, the analysis in [6] leads to the linear system

$$\begin{pmatrix} \xi_+' \\ \xi_-' \\ \eta_+' \\ \eta_-' \end{pmatrix} = \begin{pmatrix} 0 & 0 & 1 & 0 \\ 0 & 0 & 0 & 1 \\ -\omega i\alpha + \omega^2 + I_1(m) & -\omega i\alpha + I_2(m) & -\alpha - 2\omega i & \alpha \\ \omega i\alpha + I_2(m) & \omega i\alpha + \omega^2 + I_1(-m) & \alpha & -\alpha + 2\omega i \end{pmatrix} \begin{pmatrix} \xi_+ \\ \xi_- \\ \eta_+ \\ \eta_- \end{pmatrix}. \quad (24)$$

Let us remind that the perturbations are of the form $\tilde{y}_j(t) = Re^{i\theta_j}(1 + h_j(t))$, with $h_j = \xi_+(t)e^{im\theta_j} + \xi_-(t)e^{-im\theta_j}$, $m = 2, 3, \dots$, such that $|h_j| \ll 1$ and satisfying (12), with $(\eta_+, \eta_-) = (\xi_+', \xi_-')$. We will make use of (24) to study the stability of mill rings with repulsion.

4.2. **Numerical tests.** Unlike the case of flock solutions where the asymptotic speed does not play role in the linear stability, we will show that the asymptotic speed $|u_0|$ can be used as a bifurcation parameter for mills.

In Table 3 we numerically investigate the behavior of the stability region for a fixed number of particles, $N = 1000$, and for increasing values of the asymptotic speed $|u_0|$. We observe that the stability region shrinks with respect to a and gets larger with respect to b. Each stability region in Table 3 is computed out of the intersection of the stable areas for the system (24) for each perturbation mode $m \geqslant 2$. Note that for $|u_0| = 0$ the stability region coincides with the one for the the first order model (2) and for the flock ring solution.

A similar analysis, as done in Subsection 3.2, can be performed to study the formation of fat mills and clustered mill solutions. We show how both the fattening and the clustering instability are triggered by tunning the asymptotic speed for a choice of the interaction potential (a and b).

In the case of flock ring solutions we observe cluster solutions or annulus solutions when parameters a and b are chosen respectively "below" or "above" the stability region. In the case of mill solutions, a similar behavior is observed, but this will depend also on the chosen value of $|u_0|$. As an example, we fix $(a, b) = (5, 0.5)$, marked as $(\odot)$ in Table 3, and we observe the behavioral change of the system for increasing values of the asymptotic speed.

Table 4 exhibits this switching behavior from a fat mill to a cluster pattern along with the increment of the asymptotic speed. We observe that for small values of the asymptotic speed

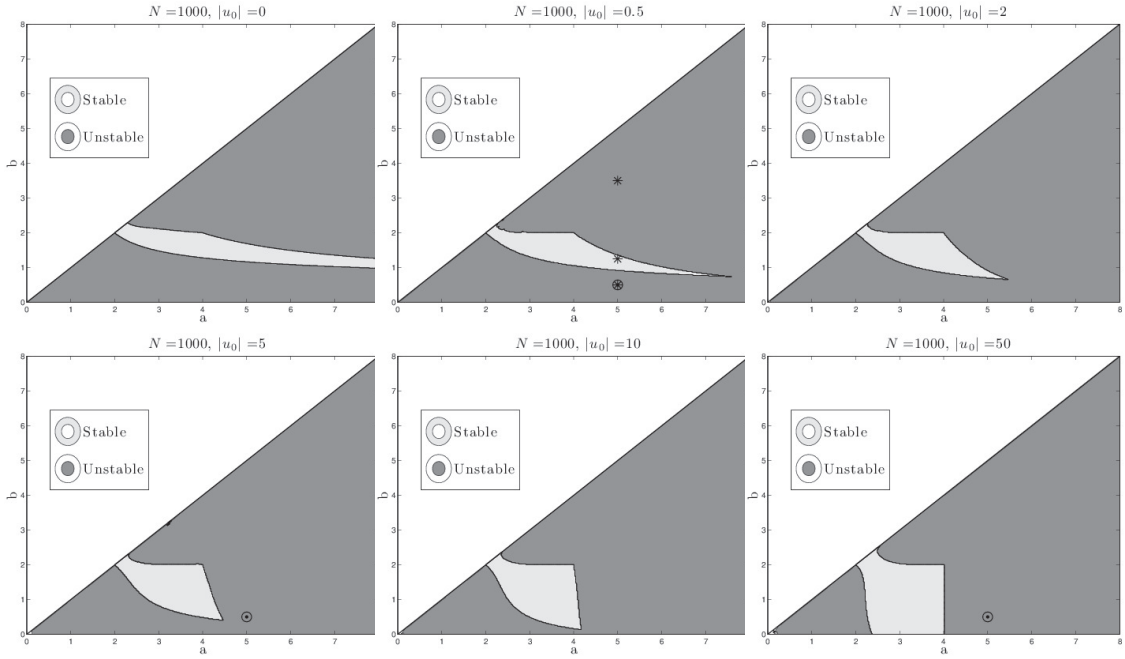

TABLE 3. Stability region for $N = 1000$ and different values of the asymptotic speed $|u_0|$. Markers ($\odot$) and ($*$) correspond to the explored parameters in Table 4 and Table 5.

fat mill solutions are stable patterns, but when increasing the value of $|u_0|$ the stable solutions form a clustered mill. The first row shows the evolution of the system with asymptotic speed $|u_0| = 0.25$ towards an annulus mill. In the second row we take $|u_0| = 0.5$ the previous stable solution is reshaped to a fat clusters pattern. The speed in the third row is switched to $|u_0| = 5$ and clusters on lines emerge as a stable configuration. Increasing the speed to $|u_0| = 50$ in the fourth row we can observe that clusters on "points" are stable solutions.

In Figure 8 we numerically show how the stability region looks like in terms of $(|u_0|, b)$, with a fixed at 0.5, and we enlighten with marker points ($\odot$) the parameter choices of Table 4, first and second lines.

For the sake of completeness, we enrich the analysis fixing $|u_0| = 0.5$ and considering different values of b, in order to cross the stability region. Therefore in Table 5 we show the evolution of a mill ring solution with b taken subsequently equal to $0.5, 1.25, 3.5$, parameter choices are marked as ($*$) in Figure 8. The first line of Table 5 shows the convergence to the same stable state as the one in second line of Table 4, but, since the system starts to evolve directly from a ring mill solution, the transient behavior is different. Parameters in second line belong to the stability region, see Figure 8. Therefore, the stable state becomes a mill ring solution. Finally, in the third line we increase b and a three point cluster solution is observed as stable pattern.

4.2.1. *Mill to Flock and Flock to Mill behavior.* We numerically investigate the stability of mill and flock ring solutions for small values of the asymptotic speed, $|u_0|$, and the parameter b, which corresponds to a strong repulsion condition.

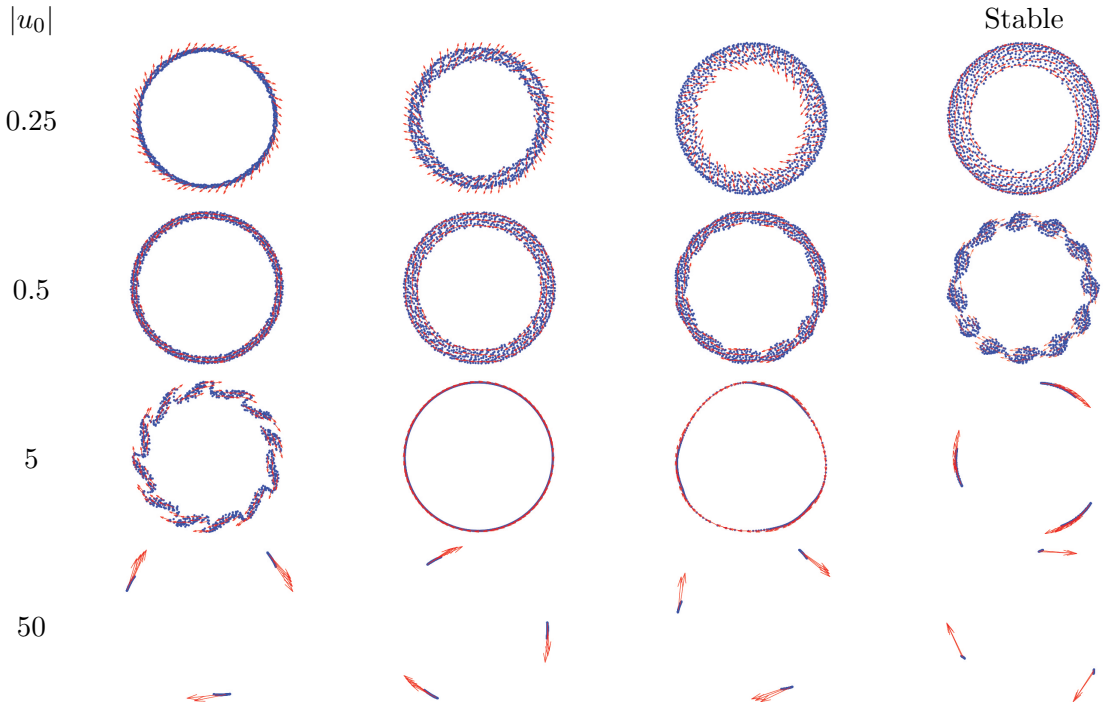

TABLE 4. $N = 1000$ particles, $a = 5, b = 0.5$. The table shows the evolution of a mill ring for increasing values of the speed $|u_0|$. Each row depicts the behavior of the system for a fixed speed, until a stable state is reached. The evolution of the second, third and fourth row is computed starting from the stable pattern of the previous line.

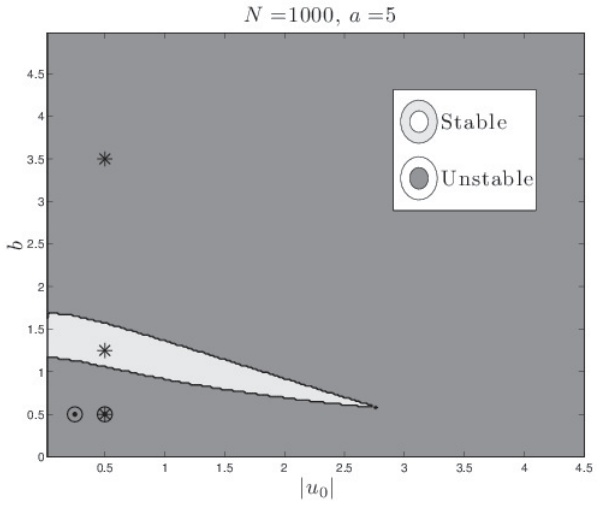

FIGURE 8. Stability region for mill ring solution with parameter $a = 5$, $N = 1000$. Markers ($\odot$) and ($\ast$) depict the parameter choices respectively for Table 4 and Table 5.

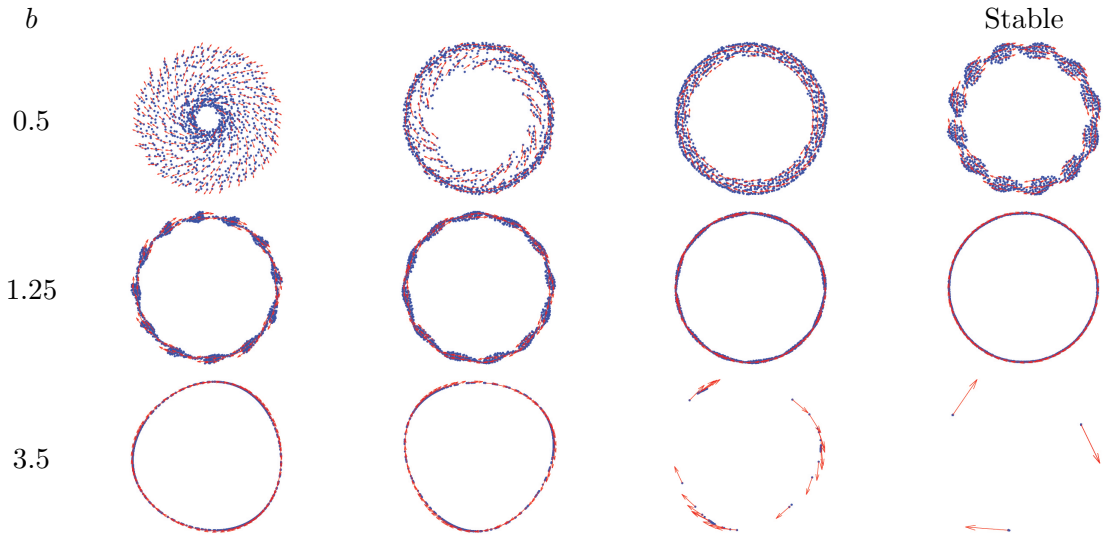

TABLE 5. $N = 1000$ particles, $a = 5, |u_0| = 0.5$. The table shows the evolution of a mill ring for increasing values of b, i.e. decreasing repulsion. The evolution of the second and the third row is computed starting from the stable pattern of the previous line.

We perform two representative simulations showing that for a particular choice of the parameters, mill ring solutions can switch to fat flock solutions and conversely flock mill solutions switch to fat mill patterns.

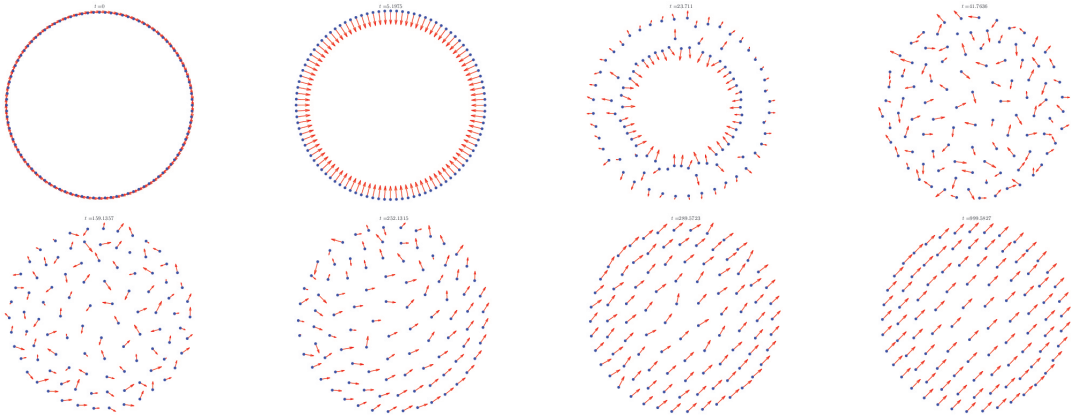

TABLE 6. System with $N = 100$ agents, parameters are fixed $a = 4$ and $b = 0.0005$ and $|u_0| = 0.01$. The first row shows that the initial mill ring configuration is unstable. The second row outlines the self organization of the system in a fat flock configuration.

In Table 6 we take $N = 100$ particles and we fix $a = 4, b = 0.0005$ and $|u_0| = 0.01$. The frames in the first row show the instability of mill ring solutions for this choice of parameters. The system initially evolves to an almost chaotic state, then particles start to organize rotating

around the center of mass. This rotation actually causes the alignment of the agents and the final fat flock configuration described in the second row. In Table 7 we consider as initial state a flock ring solution. The parameters of the model are $N = 100$, $a = 4$, $b = 0.001$ and $|u_0| = 0.1$. The first row of the table illustrates that the initial configuration is not a stable solution. Therefore, the symmetry of the flock ring is broken and the system exhibits a chaotic behavior. In the second row a rotating dynamic emerges out of the disordered state and finally the system stabilizes to a fat mill solution.

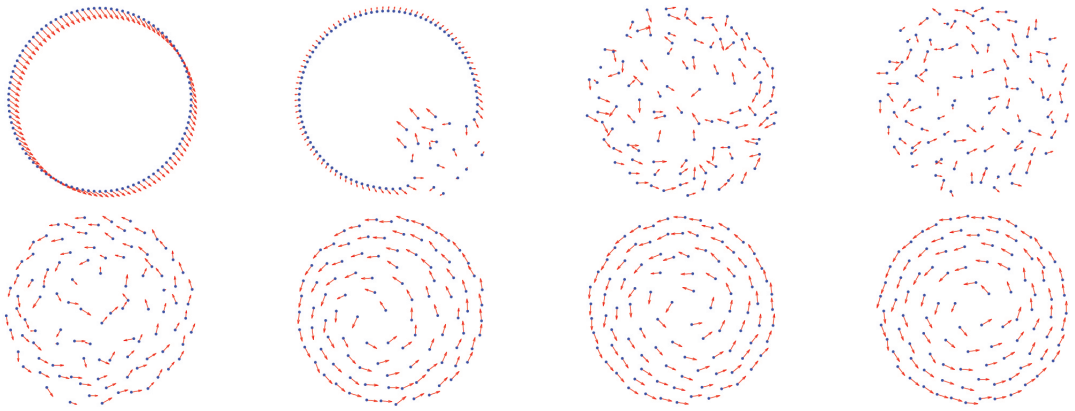

TABLE 7. System with $N = 100$ agents, parameters $a = 4$ and $b = 0.001$ and $|u_0| = 0.1$. The first row shows the instability of the flock ring solution while the second exhibits the convergence to a fat mill type solution.

These numerical tests show surprisingly that it is possible, with a particular choice of the parameters, to obtain mill configurations out of perturbations of initial flock solutions and flock solutions out of perturbations of mill ring solutions. These heteroclinic-kind solutions have not been previously reported. We also remark that the parameter choice is connected to the number of agents we are considering; changing N means finding another set of parameters for which the same switching behavior occurs.

REFERENCES

[1] I. Aoki. A simulation study on the schooling mechanism in fish. *Bull. Japan Soc. Sci. Fish*, 48:1081–1088, 1982.

[2] D. Balagué, J. A. Carrillo, T. Laurent, and G. Raoul. Dimensionality of local minimizers of the interaction energy. *to appear in ARMA*, 2013.

[3] D. Balagué, J. A. Carrillo, T. Laurent, and G. Raoul. Nonlocal interactions by repulsive-attractive potentials: radial ins/stability. *to appear in Physica D*, 2013.

[4] M. Ballerini, N. Cabibbo, R. Candelier, A. Cavagna, E. Cisbani, I. Giardina, V. Lecomte, A. Orlandi, G. Parisi, A. Procaccini, M. Viale, and V. Zdravkovic. Interaction ruling animal collective behavior depends on topological rather than metric distance: Evidence from a field study. *Proceedings of the National Academy of Sciences*, 105(4):1232–1237, 2008.

[5] A. B. T. Barbaro, K. Taylor, P. F. Trethewey, L. Youseff, and B. Birnir. Discrete and continuous models of the dynamics of pelagic fish: application to the capelin. *Math. Comput. Simulation*, 79(12):3397–3414, 2009.

[6] A. L. Bertozzi, H. Sun, J. von Brecht, T. Kolokolnikov, and D. Uminsky. Ring patterns and their bifurcations in the model of biological swarms. *Submitted*.

[7] B. Birnir. An ODE model of the motion of pelagic fish. *J. Stat. Phys.*, 128(1 - 2):535–568, 2007.

[8] S. Camazine, J.L. Deneubourg, N. R. Franks, J. Sneyd, G. Theraulaz, and E. Bonabeau. *Self-Organization in Biological Systems*. Princeton University Press, Princeton, 2001.
[9] J. A. Cañizo, J. A. Carrillo, and J. Rosado. A well-posedness theory in measures for some kinetic models of collective motion. *Math. Models Methods Appl. Sci.*, 21(3):515–539, 2011.
[10] J. A. Carrillo, M. Fornasier, J. Rosado, and G. Toscani. Asymptotic flocking dynamics for the kinetic cucker-smale model. *SIAM J. Math. Anal.*, 42:218–236, 2010.
[11] J. A. Carrillo, Y. Huang, and S. Martin. Existence, uniqueness, and orbital stability of localized flock solutions in kinetic models. *work in preparation*, 2013.
[12] J.A. Carrillo, M.R. D'Orsogna, and V. Panferov. Double milling in self-propelled swarms from kinetic theory. *Kin. Rel. Mod.*, 2:363–378, 2009.
[13] Y. Chuang, M. R. D'Orsogna, D. Marthaler, and L. Chayes A. Bertozzi. State transitions and the continuum limit for interacting, self-propelled particles. *Phys. D*, 232:33–47, 2007.
[14] F. Cucker and S. Smale. Emergent behavior in flocks. *IEEE Trans. Automat. Control*, 52(5):852–862, 2007.
[15] F. Cucker and S. Smale. On the mathematics of emergence. *Jpn. J. Math.*, 2(1):197–227, 2007.
[16] P. Degond and S. Motsch. Continuum limit of self-driven particles with orientation interaction. *Math. Models Methods Appl. Sci.*, 18(suppl.):1193–1215, 2008.
[17] M. R. D'Orsogna, Y. Chuang, A. Bertozzi, and L. Chayes. Self-propelled particles with soft-core interactions: patterns, stability and collapse. *Phys. Rev. Lett.*, 96(104302), 2006.
[18] A. Dussutour, S.C. Nicolis, J.-L. Deneubourg, and V. Fourcassié. Collective decision in ants under crowded conditions. *Behavioral Ecology and Sociobiology*, 61(17-30), 2006.
[19] S.-Y. Ha and J.-G. Liu. A simple proof of the Cucker-Smale flocking dynamics and mean-field limit. *Commun. Math. Sci.*, 7(2):297–325, 2009.
[20] S. Y. Ha and E. Tadmor. From particle to kinetic and hydrodynamic descriptions of flocking. *Kinet. Relat. Models*, 1(3):415–435, 2008.
[21] C. K. Hemelrijk and H. Hildenbrandt. Self-organized shape and frontal density of fish schools. *Ethology*, 114:245–254, 2008.
[22] A. Huth and C. Wissel. The simulation of fish schools in comparison with experimental data. *Ecol. Model.*, 75/76:135–145, 1994.
[23] A. L. Koch and D. White. The social lifestyle of myxobacteria. *BioEssays*, 20(12):1030–1038, 1998.
[24] T. Kolokolnikov, Y. Huang, and M. Pavlovski. Singular patterns for an aggregation model with a confining potential. *to appear in Physica D.*
[25] T. Kolokonikov, H. Sun, D. Uminsky, and A. Bertozzi. Stability of ring patterns arising from 2d particle interactions. *Physical Review E*, 84(1):015203, 2011.
[26] H. Levine, W.-J. Rappel, and I. Cohen. Self-organization in systems of self-propelled particles. *Phys. Rev. E*, 63:017101, Dec 2000.
[27] R. Lukeman, Y.X. Li, and L. Edelstein-Keshet. Inferring individual rules from collective behavior. *Proc. Natl. Acad. Sci. U.S.A.*, 107(28):12576–12580, 2010.
[28] J. Parrish and L. Edelstein-Keshet. Complexity, pattern, and evolutionary trade-offs in animal aggregation. *Science*, 284(5411):99 –101, 1999.
[29] T. Vicsek, A. Czirók, E. Ben-Jacob, I. Cohen, and O. Shochet. Novel type of phase transition in a system of self-driven particles. *Phys. Rev. Lett.*, 75(6):1226–1229, 1995.
[30] J. von Brecht, D. Uminsky, T. Kolokolnikov, and A. Bertozzi. Predicting pattern formation in particle interactions. *Math. Mod. Meth. Appl. Sci.*, 22:1140002, 2012.

[1]Dipartimento di Matematica e Informatica, Università di Ferrara, Ferrara 44121, Italy.
E-mail: giacomo.albi@unife.it.

[2]Departament de Matemàtiques, Universitat Autònoma de Barcelona, E-08193 Bellaterra, Spain. E-mail: dbalague@mat.uab.cat.

[3]Department of Mathematics, Imperial College London, London SW7 2AZ, UK.
E-mail: carrillo@imperial.ac.uk.

[4]Department of Mathematics, University of California - Los Angeles, Los Angeles, CA 90095, USA. E-mail: jub@math.ucla.edu.